Published in final edited form as:

Med Phys. 2019 December ; 46(12): 5444–5453. doi:10.1002/mp.13863.

Novel Acoustic Coupling Bath using Magnetite Nanoparticles for MR-Guided Transcranial Focused Ultrasound Surgery

Steven P. Allen[1], **Tom Steeves**[2], **Austin Fergusson**[3], **Dave Moore**[4], **Richey M Davis**[5], **Eli Vlaisialjevich**[3,6], **Craig H. Meyer**[1,7]

[1]Department of Biomedical Engineering, University of Virginia, Charlottesville, USA,

[2]Department of Mechanical Engineering, Virginia Tech, Blacksburg, USA,

[3]Graduate Program in Translational Biology, Medicine, and Health, Virginia Tech, Blacksburg, USA,

[4]The Focused Ultrasound Foundation, Charlottesville, USA,

[5]Department of Chemical Engineering, Virginia Tech, Blacksburg, USA,

[6]Department of Biomedical Engineering and Mechanics, Virginia Tech, Blacksburg, USA,

[7]Department of Radiology and Medical Imaging, University of Virginia, Charlottesville, USA

Abstract

Purpose: Acoustic coupling baths, nominally composed of degassed water, play important roles during transcranial focused ultrasound surgery. However, this large water bolus also degrades the quality of intraoperative magnetic resonance (MR) guidance imaging. In this study, we test the feasibility of using dilute, aqueous magnetite nanoparticle suspensions to suppress these image degradations while preserving acoustic compatibility. We examine the effects of these suspensions on metrics of image quality and acoustic compatibility for two types transcranial focused ultrasound insonation regimes: low duty cycle histotripsy procedures and high duty cycle thermal ablation procedures.

Methods: MR guidance imaging was used to monitor thermal ablations of *in vitro* gel targets using a coupling bath composed of various concentrations of aqueous, suspended, magnetite nanoparticles in a clinical transcranial transducer under stationary and flowing conditions. Thermal deposition was monitored using MR thermometry simultaneous to insonation. Then, using normal degassed water as a coupling bath, various concentrations of aqueous, suspended, magnetite nanoparticles were placed at the center of this same transducer and insonated using high duty cycle pulsing parameters. Passive cavitation detectors recorded cavitation emissions, which were then used to estimate the relative number of cavitation events per insonation (cavitation duty cycle) and cavitation dose estimates of each nanoparticle concentration. Finally, the nanoparticle mixtures were exposed to low duty cycle, histotripsy pulses. Passive cavitation detectors monitored cavitation emissions, which were used to estimate cavitation threshold pressures.

Corresponding Author: 415 Lane Road, Charlottesville, VA, USA 22908, 434-924-5101, spa5c@virginia.edu.

Disclosure

Author Eli Vlaisavljevich has a consulting relationship with HistoSonics, Inc.

Results: The nanoparticles reduced the MR signal of the coupling bath by 90% in T2 and T2*-weighted images and also removed almost all imaging artifacts caused by coupling bath motion. The coupling baths caused less than 5% changes in peak temperature change achieved during sonication, as observed via MR thermometry. At low insonation duty cycles, the nanoparticles decreased the cavitation threshold pressure by about 15 ± 7% in a manner uncorrelated with nanoparticle concentration. At high insonation duty cycles, the 0.5 cavitation duty cycle acoustic power threshold varied linearly with nanoparticle concentration.

Conclusions: Dilute aqueous magnetite nanoparticle suspensions effectively reduced MR imaging artifacts caused by the acoustic coupling bath. They also attenuated acoustic power deposition by less than 5%. For low duty cycle insonation regimes, the nanoparticles decreased the cavitation threshold by 15 ± 7%. However, for high duty cycle regimes, the nanoparticles decreased the threshold for cavitation in proportion to nanoparticle concentration.

Keywords

Magnetite; Iron Oxide; MRI; focused ultrasound; HIFU; cavitation

Introduction

Transcranial focused ultrasound (T-FUS) is a platform technology that promises noninvasive neurosurgical therapies, including thermal[1] and mechanical ablations[2], for a host of indications[3–5]. The technology's main advantages include its non-invasive nature and spatial selectivity[4]. Because T-FUS is noninvasive, surgeons rely on real-time image guidance to ensure acceptable treatment outcomes. Magnetic resonance imaging (MRI) can provide anatomical imaging, thermometry, functional assessments, and lesion identification and classification[6] and is routinely used to guide T-FUS procedures. When the quality and accuracy of MR imaging increases, the surgeon's degree of control over treatment safety and efficacy also increases[7,8].

T-FUS procedures use a large array of electronically steered acoustic transducer elements to control the deposition of acoustic energy into the brain[9]. These elements sit on a rigid, hemispherical frame whose surface, due to geometrical constraints, stands several centimeters off of the patient's scalp. To improve acoustic transmittance, protect the patient's scalp against surface burns, and minimize the occurrence of unwanted cavitation, clinical implementations of T-FUS circulate this space with a chilled degassed coupling bath[10]. Degassed water remains the most commonly used coupling bath because it is inexpensive, readily conveys heat, possesses a similar acoustic impedance to soft tissues, and does not easily absorb or shock the acoustic pulses as they propagate.

While vital to acoustic transmission, this bath also contributes to imaging errors during intraoperative MR scanning. For example, the coupling bath requires a large imaging field of view, thereby increasing image acquisition times and limiting the maximum sampling rate of a thermometry time course. The bath's large relative signal magnitude can skew the MR scanner's prescan algorithm to favor image quality in the coupling bath. Poor calibration leads to blurred or shifted images and degraded signal levels and tissue contrasts in the patient[11]. Meanwhile, continuous circulation and degassing would decrease heating in the

patient's scalp and skull and may also reduce the chance of unwanted cavitation in the coupling bath. However, it is currently impossible to cool and degas the coupling bath while using MRI to monitor a sonication because water movement produces data inconsistencies across MRI's piecewise image sampling process, resulting in imaging errors. Examples of these imaging artifacts are displayed in Figure 1. A coupling bath that could remove these sources of imaging error and also enable continuous cooling and degassing during sonication would improve the reliability and accuracy of MR guidance imaging during T-FUS procedures.

In an effort to remove similar artifacts associated with a focused ultrasound device dedicated to breast ablations, Deckers et al.[12] and Merckel et al.[13] dissolved manganese chloride into a partitioned subsection of the coupling bath volume immediately in contact with the patient. The manganese accelerated the coupling bath's transverse relaxation process, rendering it, when sampled at late echo times, too small relative to the patient's MR signal to produce major imaging artifacts. The device also employed localized imaging coils to reduce image sensitivity to the manganese-free partition of the water bath. While effective for the dedicated breast device, dissolved manganese chloride remains suboptimal for use in T-FUS because the size of the transducer forces one to use receiver coils that are sensitive to the entire volume of the coupling bath. Filling the entire bath with dissolved salts would expose the transducer surface to corrosive materials, reduce the electrical isolation between the patient from the transducer hardware, and considering the 7–12 L volume of the water bath, introduce a non-trivial source of image noise.

Here, we propose replacing manganese chloride with aqueous suspensions of superparamagnetic magnetite nanoparticles. Previous work has shown that particles of encapsulated magnetite efficiently accelerate the MR transverse relaxation process[14–16]. They can also be made electrically neutral, chemically stable[17], and biocompatible[18], and their high relaxivity permits very dilute concentrations. For example, an aqueous, 1 mM magnetite concentration suspension should accelerate the coupling bath's R_2 rate from its native 0.3 s^{-1} to 100 s^{-1} while only altering its density, and thus its acoustic impedance, by 0.02%. We hypothesize that, when used as an acoustic coupling medium during a T-FUS procedure, these suspensions will simultaneously preserve acoustic coupling and rapidly decay the bath's MR signal, rendering it too small relative to the patient's MR signal to produce major imaging artifacts and allow continuous circulation. Further, unlike other candidate coupling baths—such as deuterated water, perfluoropolyethers and oils, and chelated contrast agents—magnetite is abundant, inexpensive, and, at dilute concentrations, does not alter acoustic attenuation, fluid viscosity, heat convection, or fluid conductivity.

Two remaining important acoustic compatibility aspects are the chance that the nanoparticles will enhance acoustic cavitation or heating in the coupling bath. It is widely known that impurities promote cavitation activity in water[19,20]. Enhanced acoustic cavitation in the coupling bath would be undesirable because it can block acoustic transmission, damage the surfaces of the transducer and the scalp, and falsely signal that cavitation has occurred within the patient. Meanwhile, enhanced heating in the water bath or on the patient's skin would promote skin burns. Several previous reports have examined potential acoustic interactions between magnetite nanoparticles and focused ultrasound. Work by

Smith et al.[21] and Ho et al.[22] found that aqueous, aggregated magnetite particles seed cavitation nuclei upon insonation. Meanwhile, Sun et al.[23] and Wang et al.[24] found that injected, surface-modified magnetite particles enhanced the efficacy of continuous wave HIFU treatments in ex vivo liver and rabbit and in vivo murine cancer models, which was attributed to enhanced acoustic absorption. However, it is not possible to use these studies to predict the prevalence of nanoparticle-enhanced cavitation or heating in our desired application. For example, Smith et al.[21], Sun et al.[23], and Wang et al.[24] were not able to report the concentration of the magnetite nanoparticles at the insonation site. Meanwhile, Ho et al.[22] insonated nanoparticle concentration of 116 mM, which is two orders of magnitude larger than necessary for our purposes. Smith et al.[21] and Ho et al.[22] used acoustic pulsing duty cycles of 0.5–50%, which differ from the 100% and <0.1% duty cycles associated with T-FUS thermal and mechanical ablations (histotripsy), respectively. Finally, Sun et al.[23] and Wang et al.[24] did not quantify cavitation activity, which does not preclude the possibility of cavitation-enhanced heating[25].

In this study, we examine the feasibility of using dilute, aqueous magnetite nanoparticle suspensions as an acoustic coupling bath for T-FUS. We first examine the ability of these nanoparticles to suppress the MR signal of the coupling bath and alleviate motion artifacts on MR guidance imaging during an in vitro T-FUS procedure. We then examine their impact on heat deposition in an in vitro gel target. Finally, we examine their impact on cavitation threshold metrics under T-FUS thermal (100% duty cycle) and mechanical (<0.1% duty cycle) ablation insonation schemes.

Materials and Methods

Magnetite Nanoparticles and Characterization

Aqueous, magnetite nanoparticles with an advertised 99.5% purity were purchased from a commercial vendor (Stock# US7568, US Research Nanomaterials, Houston, TX). Nanoparticle size was determined with dynamic light scattering (DLS). Briefly, the purchased nanoparticles were diluted in deionized water (18 megOhm resistivity) and then sonicated for 30 minutes in an ultrasonic water bath (Model# 15337410, Fisher Scientific, Suwanee, GA). DLS measurements were then performed at 25 °C using a Malvern Zetasizer Nano-ZS and the Malvern Zetasizer Software (v7.12). While the particle size was advertised to be 20 nm, dynamic light scattering revealed that the particles agglomerated in water with a mean intensity-average diameter of 240 nm, a similar value to that reported in Smith et al.[21] and Ho et al[22]. The particle size distribution measured by DLS was monomodal with a polydispersity index ~ 0.4 and did not change with sonication time up to 30 minutes. The advertised concentration of 20% w/wt was assumed to be correct and all material was assumed to have a Fe_3O_4 chemical composition. The particles demonstrated an R2 relaxivity of 526 s^{-1} mM^{-1} when examined using standard multi-spin-echo measurements on a 3T MRI scanner (MR 750, General Electric, Waukesha, WI) which is much larger than the value of 93 s^{-1} mM^{-1} reported for a commercial magnetite-based contrast medium (Feridex/Endorem) in water at 37 °C and 3T[26]. In the experiments described below, various coupling baths were formed by diluting the purchased nanoparticles in degassed water. Due to aggregation, the particles would begin settling within 20 minutes after suspension and care

was taken to either continuously circulate or periodically resuspend the solutions over the course of each experiment.

Experiment 1: MR Imaging

To test the ability of the particles to suppress the coupling bath's MR signal, a 30 cm, 1024 element, 650 kHz transducer array (Insightec Exablate Neuro, Haifa Israel), was oriented "face up" with its bowl concave toward the ceiling and filled with aqueous nanoparticle concentrations ranging from 0–0.49 mM. A small polyacrylamide gel phantom was placed at the transducer focus and scanned using anatomical T2-weighted sequences and thermometry sequences common to T-FUS procedures. The thermometry scans were performed using a single-slice, multi-echo gradient-echo sequence (GRE, repetition time: 28 ms, field of view: 28 cm, matrix size: 256×128 pixels, bandwidth: 35.7 kHz, echo times: 3.3, 8.0, 12.8, 17.6, and 22.4 ms, frame rate: 3.5 s). The T2-weighted sequences were either a 2D, multi-slice, half-Fourier acquisition, single shot, turbo-spin-echo sequence (HASTE, repetition time: 4.6 s, echo time: 81 ms, echo train length: 88, field of view: 24×24 cm, matrix size: 384×160 pixels, slice thickness: 8 mm, bandwidth: 325 kHz) or a 2D, multi-slice, turbo-spin echo sequence (TSE, repetition time: 7.7 s, echo time: 81 ms, echo train length: 24, field of view: 32 cm, matrix size: 256×256 pixels, slice thickness: 3 mm, bandwidth: 195 kHz). To prevent particle settling, the water was continuously circulated using a small pump for all acquisitions except for one turbo-spin echo image acquired with a stationary 0 mM nanoparticle concentration coupling bath. This experimental setup is depicted schematically in Figure 2-A.

Experiment 2: Thermal Deposition

In this experiment, we tested the ability of the particles, as a coupling bath, to attenuate thermal deposition of ultrasound in a target gel. The 30 cm, 1024 element transducer used in Experiment 1 was oriented "face up" and its bowl was filled aqueous nanoparticle concentrations of 0 or 0.25 mM. A small, hemispherical, plastic holder (acoustic attenuation less than 0.18 dB, volume of 250 mL) was placed at the transducer focus. This holder was filled with a gel with an acoustic absorbance of less than 0.0012 Np mm^{-1} (Aquaflex, Parker Laboratories, Fairfield, NJ) and repeatedly insonated for 10s at acoustic powers ranging from 50 to 600 W. Insonations at each power level were repeated three times with approximately four minute delays between each instance to allow for sample cooling. The GRE MR thermometry sequence described in Experiment 1 was used, simultaneous to insonation, to monitor heating in the gel target. To prevent settling, the coupling baths with nanoparticle concentrations greater than 0 mM were continuously circulated using a pump and hosing apparatus. This experimental setup is depicted schematically in Figure 2-A.

Experiment 3: Cavitation Threshold During High Duty cycle Insonation

The transducer used in experiments one and two was again oriented "face up" and filled with degassed water. A small, hemispherical, polystyrene shell with 1 mm wall-thickness (acoustic attenuation less than 0.18 dB, volume of 115 mL) was placed at the focus and filled with aqueous magnetite nanoparticles ranging in concentration from 0 to 0.5 mM Fe_3O_4. An acoustic absorber (Aptflex F48, Precision Acoustics, Dorchester, UK) was then placed on top of the plastic holder to both attenuate acoustic reflections at the air-fluid

interface and to prevent surface vibrations. The transducer then deposited 10 s duration, continuous wave sonications with acoustic powers ranging from 1 to 250 W into the holder. Because all sonications could be completed in less than 5 minutes and excess sediment was not observed at the bottom of the holder after each experiment, we did not periodically perturb or resuspend the particles after initial mixture. This experiment is depicted schematically in Figure 2-B.

Cavitation detection was accomplished using eight wideband passive cavitation detectors (PCD) built into the transducer device. These detectors sampled the ambient acoustic emissions at a rate of 2 MHz for a 10 ms period and employed a passive, low-pass filter with a −6 dB cutoff frequency near 500 kHz. The system continuously collected data, producing approximately 1020 spectra per 10 s insonation. The Fourier transforms of the sampled emissions were then exported to a personal computer and analyzed using custom routines written in MATLAB (The MathWorks, Natick, MA). Specifically, spectra from all eight receivers (which were very similar in magnitude and shape) were first averaged together and the root mean square average (RMSA) of the 60–500 kHz band of each spectra was computed. Baseline spectral behavior was computed by taking the mean and standard deviation of the RMSA estimates from the 1 W insonation of the 0 mM nanoparticle concentration sample. During all other insonations, a cavitation event was assumed to occur when the RMSA value of a spectrum exceeded this baseline mean by more than 5 standard deviations. The cavitation duty cycle was then computed as the fraction of spectra acquired during an insonation that satisfied this criterion. The resulting curves were then fit to a Gaussian cumulative distribution function. Finally, the inertial cavitation dose of a given sonication was estimated by summing together the RMSA estimates associated with each insonation[27]. For comparison with the low-duty cycle regime, the 0.5 cavitation duty cycle power thresholds returned by the fit were converted to pressure (P) using the formulation $P = \sqrt{P_a z / A}$, where P_a is the acoustic power, z is the acoustic impedance of water ($1.48 * 10^6$ Rayls), and A is the transducer's focal area (2.545 mm^2), as supplied by the manufacturer.

Experiment 4: Cavitation Threshold During Low Duty cycle Insonation

A 700 kHz, shock-scattering histotripsy transducer[28](Histosonics, Ann Arbor, Michigan) was used to examine the propensity of the particles to seed cavitation under a low duty cycle insonation regime. The transducer consisted of 36 elements arranged in a 13 cm aperture and an 11 cm focal distance. Aqueous magnetite particles with concentrations of 0–0.36 mM were then used to fill a custom, water-proof chamber designed with both an acoustically transparent window as well as optical windows to allow high speed videography. The center of the chamber was placed at the transducer focus and the entire setup was immersed in a tank of degassed, circulating water. The transducer then deposited 100 highly focused, shocked, 5 cycle pulses into the chamber at a pulse rate of 1 Hz (duty cycle of 0.0007%). The window attenuated the acoustic pulses by −0.13 dB. This experiment was repeated as the peak negative pressures of the acoustic pulses ranged from −8 to −42 MPa, which encompassed the range of pressures over which we observed cavitation activity. To prevent settling, the chamber was gently rotated after every other instance where the acoustic pressure was altered, a period of approximately every 5 minutes. One of the 36 elements was

connected to an oscilloscope through a cable splitter and a 100× attenuator and used as a PCD system in a similar manner as has been reported elsewhere[29,30]. This experiment is depicted schematically in Figure 2-C.

Because the opacity of the coupling bath varied with nanoparticle concentration, optical images could not be reliably used to detect cavitation events over all experiments reported here. Instead, the camera was used to calibrate the PCD system in the following manner. First, the oscilloscope was triggered to only record voltage fluctuations across the transducer element at times corresponding to acoustic propagation across twice the transducer's focal distance. Then, with the chamber filled with degassed water, the negative pressures of the acoustic pulses were increased until cavitation events could be consistently detected on optical photographs. The voltage threshold used to determine a cavitation event while during insonation of any coupling bath was then taken to be 80% of the peak recorded voltage on the oscilloscope after averaging over 4 calibration experiments.

For each nanoparticle concentration, the fractions of PCD voltages above the detection threshold were computed and fitted, as a function of peak negative pressure and via a least-squares algorithm, to a Gaussian cumulative distribution in the same manner as published elsewhere[31,32]. This fitted curve was then taken to express the relative probability of a cavitation event as a function of exposure to a pulse at a given peak negative pressure.

Results

Experiment 1:

Example images of a gel target acquired with the fast-spin-echo and gradient-echo sequence are displayed in Figure 3 for two different nanoparticle concentrations within the coupling bath. At the echo-times listed in the figure, a 0.25 mM nanoparticle concentration was able to suppress 90% of the coupling bath relative to degassed water. Figure 3 also plots the magnitude of the coupling bath signal relative to that of the gel target as a function of particle concentration. While no attempt at fitting has been made, the signal magnitude roughly follows a multi-exponential decay pattern. Further, we observed that the largest magnitude of signal suppression occurs at the jump between 0 and 0.6 mM nanoparticle concentrations, with decreasing step sizes as nanoparticle concentration increases. We expect the exact nature of this curve to vary with the echo spacing used to make the measurement.

Example images from the HASTE sequences are displayed in Figure 4 for three different nanoparticle concentrations within the coupling bath. These images display motion artifacts in both the coupling bath itself and the gel target that reduce with nanoparticle concentration. Figure 4 also plots the standard deviation of an ROI centered on the portion of the gel target subjected to visible motion artifact, normalized by the average signal intensity of the portion of the gel not subject to visible motion artifact. At 0 mM nanoparticle concentration, the standard deviation of the signal in the ROI is 30% that of the mean gel signal intensity. Higher nanoparticle concentrations reduce this parameter to 5% of the mean gel signal intensity. Similar to that shown in Figure 3, the majority of the motion artifact is removed with the smallest tested nanoparticle concentration.

Experiment 2:

The mean and standard deviation of the maximum change in temperature (averaged over a 9-voxel square window centered on the hottest voxel) achieved in the gel phantom across all 3 sonications are plotted in Figure 5 as a function of acoustic power and nanoparticle concentration. At a given power and coupling bath composition, the average temperature increase varied by 2–3 °C —a value that is larger than the 1 °C precision of the thermometry sequence. On average, sonications transmitting through the 0.25 mM nanoparticle concentration coupling bath achieved 1–3 degree lower peak temperature increase than identical sonications using a water coupling bath. Finally, while not shown in a figure, PCD traces reported enhanced RMSA levels during sonications with acoustic powers greater than 50 W when using the 0.25 mM concentration coupling bath. This phenomenon was not observed while using the 0 mM coupling bath.

Experiment 3:

Example curves of the cavitation duty cycle are plotted, along with least-squares fits to a Gaussian cumulative distribution function, in Figure 6-A as a function of acoustic power and nanoparticle concentration. All nanoparticle solutions demonstrated a monotonically increasing cavitation duty cycle and are well described by the fitting function. Nanoparticle concentrations greater than 0 mM shifted these curves toward lower acoustic powers. This behavior is most compactly expressed by the 0.5 duty cycle parameter returned by the fitting algorithm and is plotted as a function of nanoparticle concentration in Figure 6-B. The 0.5 threshold in this case decreases linearly with acoustic power with a least-squares-derived slope of 308 WmM^{-1} nanoparticle concentration. These same thresholds, converted to pressure, are displayed in Figure 7-B.

The temporal distribution of spectra satisfying the cavitation criterion appeared to mimic the behavior of a binomial random process. For example, at acoustic powers well below the 0.5 threshold, the few spectra satisfying the cavitation criterion appeared sprinkled randomly in time. As the acoustic power increased or the nanoparticle concentration increased, the relative proportion of spectra detecting a cavitation event also increased but continued to follow no obvious temporal pattern. Finally, we observed, in instances where a cavitation event was detected, that the relative magnitude of the corresponding RMSA increased with nanoparticle concentration. This effect can be observed in Figure 6-C, which plots the estimated cavitation dose of each sonication as a function of acoustic power and nanoparticle concentration.

Experiment 4:

Example plots of the observed fraction of acoustic pulses that produced detected cavitation events, along with least-squares fits to a Gaussian cumulative distribution function, are shown in Figure 7-A. All nanoparticle solutions demonstrated monotonically increasing cavitation probabilities as a function of peak negative pressure, with distinct transitions from a 0% cavitation fraction to a 100% cavitation fraction observed at peak negative pressure levels between −18 and −30 MPa. All data sets were well described by the Gaussian cumulative distribution function. Nanoparticle concentrations greater than 0 mM shifted these curves toward lower negative pressure values. This behavior is most compactly

expressed by the 0.5 cavitation probability parameter returned by the fitting algorithm and is plotted, as a function of nanoparticle concentration, in Figure 7-B. For comparison, the power thresholds in Figure 6-B are converted to acoustic pressure and also displayed. The nanoparticles decrease this threshold by an average and range of 15 ± 7%. Unlike the results from Experiment 3, these thresholds displayed too much variability to confidently determine a mathematical relationship with pressure. Finally, the smallest magnitude peak negative pressure that produced a detectable cavitation event was −22 MPa for all tested concentrations (including 0 mM) except 0.24 mM—which demonstrated a smallest magnitude pressure of −15 MPa.

Discussion

The experimental study presented above examines the feasibility of using dilute, aqueous suspensions of commercially available magnetite nanoparticles as a means to reduce the degradative effects of the acoustic coupling bath on MR guidance imaging during T-FUS procedures. Our experiments tested the acoustic compatibility of these suspensions at likely T-FUS insonation frequencies (650 and 750 kHz) and their impact on MR guidance imaging while sonicating a gel phantom. Experiment 1 demonstrated the ability of the nanoparticles to both reduce the signal magnitude of the coupling bath and remove associated motion artifacts for a broad range of dilute nanoparticle concentrations. Experiment 2 showed that a dilute nanoparticle concentration coupling bath imparted less than 5 % loss in thermal deposition over a broad range of acoustic powers and also promoted detectable cavitation activity. Experiment 3 demonstrated that, under a high duty cycle, continuous wave insonation regime, the particles reduce the 0.5 cavitation duty cycle power threshold by 308 W per each mM of nanoparticle concentration. Finally, experiment 4 indicated that these particles reduce the 0.5 probability cavitation pressure threshold when exposed to a low duty cycle, histotripsy insonation regime. Variability in the estimated pressure thresholds prevented us from confidently determining a mathematical relationship with pressure.

The main concern over the use of aqueous magnetite nanoparticles as a coupling bath is that the particles will enhance losses as an acoustic wave propagates. Losses via direct scatter off the particles, impedance mismatch, and absorption can be minimized by suspending as few particles as possible within the coupling bath. However, widespread cavitation throughout the prefocal field can also potentially block the propagation of acoustic energy into a desired target. In addition, in a clinical setting, cavitation emissions can act as important safety signals and be used to prevent tissue damage. Therefore, controlling cavitation in the prefocal acoustic field should be an important design consideration for magnetite infused acoustic coupling bath. In the case of low duty cycle insonations used in histotripsy, large negative pressures at the focus are primarily obtained by geometric focal gains using a hemispherical transducer and the acoustic pressures in the coupling bath can be expected to remain small compared to the cavitation threshold pressures observed in experiment 4. However, if treatment targets lie near the skull[33], the prefocal field in the coupling bath may approach that at the focus in order to surmount acoustic losses in the bone and cavitation in the coupling bath can become quite likely. For these cases, future coupling bath designs should consider the possibility of very large pressure fields within the bath.

In the case of high duty cycle thermal ablation procedures, care must be taken that the power deposition in the prefocal field does not approach the 0.5 cavitation duty cycle threshold. This relationship will place limitations on the acceptable maximum nanoparticle concentration for a given sonication power level. The temperature measurements described in Experiment 2 indicate that, in our system, the prefocal field remained sufficiently below the 120 W threshold associated with a 0.25 mM concentration coupling bath to impede thermal deposition by no more that 5%. It is entirely possible that higher nanoparticle concentrations will induce more spatially and temporally abundant cavitation and more seriously impede thermal buildup in the target. One limitation of this study is its lack of thermal measurements over a broader range of particle concentrations.

A second concern over using magnetite nanoparticles is settling. So long as the nanoparticle concentration is sufficiently large to remove motion artifacts, settling can easily be avoided by continuously circulating the water bath during scanning. However, it is possible that some applications, such as a histotripsy ablation near the skull surface, require a low nanoparticle concentration, which may lead to residual water motion artifacts. In these cases, it will be desirable to have the water bath stationary during MR imaging. If the imaging time lasts longer than 5 minutes, particle settling may begin to produce spatially varying suppression of the coupling bath or sufficiently increase the concentration of particles to induce high rates of cavitation. It may be possible to mitigate these effects by intermittently perturbing the water bath over the course of imaging.

A future direction of study is indicated by Smith et al.[21], who found that coating magnetite nanoparticles with silica can increase the cavitation threshold pressure. Surface modifications may be an intriguing method to reduce the chance of cavitation activity during continuous-wave sonications. However, they can also reduce the relaxivity of magnetite particles, reducing their ability to suppress the MR signal of the coupling bath[16]. Another future direction of study would be using cavitation deletion pulses to coalesce or dissolve potential nuclei[34] among the nanoparticles either before or after mixture with degassed water.

While there are a number of alternative methods to suppress the MR signal of the coupling bath, including chelated contrast agents, inversion recovery MR pulse sequences, and spatially selective RF pulses, the use of magnetite particles remains particularly attractive for several reasons. First, the rate of signal loss from the coupling bath, for a fixed echo time and repetition rate, is maximized at low nanoparticle concentrations. This relationship ensures that even very dilute solutions can suppress a large amount of imaging artifacts, better preserving, relative to chelated contrast agents, the favorable mechanical, acoustic, thermal, and electrical properties of water as a coupling bath. Second, the performance of the nanoparticles is invariant with large magnetic field and RF inhomogeneities that would reduce the efficacy of spatially-selective RF pulses. Third, while the magnetite nanoparticles will not prove beneficial to images acquired with very short echo times, they remain compatible with a wider variety of acquisition parameters and techniques than inversion recovery techniques, including rapid, gradient-echo sequences commonly used for thermometry.

Under some circumstances, it is desirable to observe the coupling bath on MRI. For example, to prevent unwanted cavitation or heating, it is important to deactivate transducer elements whose beam path intersects air pockets such as bubbles lodged on the patient's scalp or folds in the rubber membrane used to prevent the coupling bath from spilling out. In nominal practice, the bright coupling bath observed on a T2-weighted scan can nicely delineate these features. However, using the proposed nanoparticle-infused coupling bath would eliminate strong T2-weighted contrast between an air pocket and the coupling bath and prevent easy detection. A potential solution could be to use short TE scans during this phase of treatment preparation to capture the coupling bath prior to decay.

One limitation of this study is that it does not cover the full range of acoustic frequencies that may be used in T-FUS procedures. Acoustic absorption and scatter can vary with insonation frequency[35]. Studies across a spectrum of frequencies may better characterize the nature and origin of any absorption or scatter caused by the nanoparticles. A second limitation is that the delays between insonations in Experiment 3 are too short to allow complete cooling, which likely has contributed to large heating variations at several acoustic powers. A more rigorous analysis of the sound speed, attenuation, and impedance of the coupling media is likely required to accurately predict expected temperature losses while using a nanoparticle-infused coupling bath. Our study also does not examine the effect of the magnetite nanoparticles on the T1 of the coupling bath nor does it examine imaging benefits gained by using T1-weighted imaging techniques, which are an important class of neuroimaging methods.

Conclusion

This study examines the feasibility of using dilute, aqueous suspensions of commercially available magnetite nanoparticles as an acoustic coupling bath during transcranial focused ultrasound surgeries. The results show that, at dilute concentrations, these nanoparticles can effectively reduce MR signal from the coupling bath for a broad class of T2- and T2*-weighted scans without causing serious losses in heating during sonication. Meanwhile, experiments using both high and low duty cycle insonation regimes demonstrated that the particles can reduce cavitation thresholds by at least 15%. Under a high duty cycle regime, this reduction is particularly pronounced and scales linearly with particle concentration. These results suggest that magnetite nanoparticle suspensions are a feasible means to resolve MR image artifacts induced by the acoustic coupling bath during transcranial focused ultrasound surgeries so long as the prefocal acoustic field and nanoparticle concentration can be constrained below the appropriate cavitation threshold.

Acknowledgements

This work was supported, in part, by the Ivy Biomedical Innovation Fund.

Research reported in this publication/presentation/work was supported, in part, by the National Center for Advancing Translational Sciences of the National Institutes of Health under Award Number UL1TR003015. The content is solely the responsibility of the authors and does not necessarily represent the official views of the National Institutes of Health.

The authors would like to thank the Virginia Tech Department of Biomedical Engineering and Mechanics, the Institute for Critical Technology and Applied Science, the Center for Engineering Health, and the Translational Biology, Medicine, and Health Program at Virginia Tech for their support of this work

References

1. Elias WJ, Lipsman N, Ondo WG, et al. A Randomized Trial of Focused Ultrasound Thalamotomy for Essential Tremor. N Engl J Med. 2016;375(8):730–739. doi:10.1056/NEJMoa1600159 [PubMed: 27557301]
2. Sukovich JR, Cain CA, Pandey AS, et al. In vivo histotripsy brain treatment. J Neurosurg. October 2018:1–8. doi:10.3171/2018.4.JNS172652
3. Ghanouni P, Pauly KB, Elias WJ, et al. Transcranial MRI-Guided Focused Ultrasound: A Review of the Technologic and Neurologic Applications. Am J Roentgenol. 2015;205(1):150–159. doi:10.2214/AJR.14.13632 [PubMed: 26102394]
4. Ellis S, Rieke V, Kohi M, Westphalen AC. Clinical applications for magnetic resonance guided high intensity focused ultrasound (MRgHIFU): Present and future. J Med Imaging Radiat Oncol. 2013;57(4):391–399. doi:10.1111/1754-9485.12085 [PubMed: 23870333]
5. Colen RR, Sahnoune I, Weinberg JS. Neurosurgical Applications of High-Intensity Focused Ultrasound with Magnetic Resonance Thermometry. Neurosurg Clin N Am. 2017;28(4):559–567. doi:10.1016/j.nec.2017.05.008 [PubMed: 28917284]
6. Hectors SJCG, Jacobs I, Moonen CTW, Strijkers GJ, Nicolay K. MRI methods for the evaluation of high intensity focused ultrasound tumor treatment: Current status and future needs. Magn Reson Med. 2016;75(1):302–317. doi:10.1002/mrm.25758 [PubMed: 26096859]
7. Hectors SJCGCG, Jacobs I, Moonen CTWW, Strijkers GJ, Nicolay K. MRI methods for the evaluation of high intensity focused ultrasound tumor treatment: Current status and future needs. Magn Reson Med. 2015;317(1):n/a-n/a. doi:10.1002/mrm.25758
8. Ghanouni P, Pauly KB, Elias WJ, et al. Transcranial MRI-guided focused ultrasound: A review of the technologic and neurologic applications. Am J Roentgenol. 2015;205(1):150–159. doi:10.2214/AJR.14.13632 [PubMed: 26102394]
9. Hynynen K, Jones RM. Image-guided ultrasound phased arrays are a disruptive technology for non-invasive therapy. Phys Med Biol:1–50. doi:10.1088/0031-9155/61/17/R206
10. Chang WS, Jung HH, Kweon EJ, Zadicario E, Rachmilevitch I, Chang JW. Unilateral magnetic resonance guided focused ultrasound thalamotomy for essential tremor: practices and clinicoradiological outcomes. J Neurol Neurosurg Psychiatry. 2015;86(3):257–264. doi:10.1136/jnnp-2014-307642 [PubMed: 24876191]
11. Odéen Henrik; Patil Sunil; Bolster Bradley; Bhat Himanshu; Parker DL. Evaluation and tradeoffs of 2D and 3D Cartesian MR temperature imaging (MRTI) for brain applications In: 6th International Symposium on Focused Ultrasound. Reston, VA; 2018:BR–46.
12. Deckers R, Merckel LG, Denis de Senneville B, et al. Performance analysis of a dedicated breast MR-HIFU system for tumor ablation in breast cancer patients. Phys Med Biol. 2015;60(14):5527–5542. doi:10.1088/0031-9155/60/14/5527 [PubMed: 26133986]
13. Merckel LG, Knuttel FM, Deckers R, et al. First clinical experience with a dedicated MRI-guided high-intensity focused ultrasound system for breast cancer ablation. Eur Radiol. 2016;26(11):4037–4046. doi:10.1007/s00330-016-4222-9 [PubMed: 26852219]
14. Gillis P, Koenig SH. Transverse relaxation of solvent protons induced by magnetized spheres: application to ferritin, erythrocytes, and magnetite. Magn Reson Med. 1987;5(4):323–345. doi:10.1002/mrm.1910050404 [PubMed: 2824967]
15. Lee N, Hyeon T. Designed synthesis of uniformly sized iron oxide nanoparticles for efficient magnetic resonance imaging contrast agents. Chem Soc Rev. 2012;41(7):2575–2589. doi:10.1039/c1cs15248c [PubMed: 22138852]
16. Carroll MRJ, Huffstetler PP, Miles WC, et al. The effect of polymer coatings on proton transverse relaxivities of aqueous suspensions of magnetic nanoparticles. Nanotechnology. 2011. doi:10.1088/0957-4484/22/32/325702

17. Goff JD, Huffstetler PP, Miles WC, et al. Novel phosphonate-functional poly(ethylene oxide)-magnetite nanoparticles form stable colloidal dispersions in phosphate-buffered saline. Chem Mater. 2009;21(20):4784–4795. doi:10.1021/cm901006g
18. Pothayee N, Balasubramaniam S, Pothayee N, et al. Magnetic nanoclusters with hydrophilic spacing for dual drug delivery and sensitive magnetic resonance imaging. J Mater Chem B. 2013. doi:10.1039/c2tb00275b
19. Apfel RE. The Role of Impurities in Cavitation-Threshold Determination. J Acoust Soc Am. 1970;48(5B):1179–1186. doi:10.1121/1.1912258
20. Crum LA. Tensile strength of water. Nature. 1979;278(5700):148–149. doi:10.1038/278148a0
21. Smith MJ, Ho VHB, Darton NJ, Slater NKH. Effect of Magnetite Nanoparticle Agglomerates on Ultrasound Induced Inertial Cavitation. Ultrasound Med Biol. 2009;35(6):1010–1014. doi: 10.1016/j.ultrasmedbio.2008.12.010 [PubMed: 19251358]
22. Ho VHB, Smith MJ, Slater NKH. Effect of magnetite nanoparticle agglomerates on the destruction of tumor spheroids using high intensity focused ultrasound. Ultrasound Med Biol. 2011;37(1): 169–175. doi:10.1016/j.ultrasmedbio.2010.09.007 [PubMed: 21084159]
23. Sun Y, Zheng Y, Ran H, et al. Superparamagnetic PLGA-iron oxide microcapsules for dual-modality US/MR imaging and high intensity focused US breast cancer ablation. Biomaterials. 2012;33(24):5854–5864. doi:10.1016/j.biomaterials.2012.04.062 [PubMed: 22617321]
24. Wang Z, Qiao R, Tang N, et al. Active targeting theranostic iron oxide nanoparticles for MRI and magnetic resonance-guided focused ultrasound ablation of lung cancer. Biomaterials. 2017;127:25–35. doi:10.1016/j.biomaterials.2017.02.037 [PubMed: 28279919]
25. Sokka SD, King R, Hynynen K. MRI-guided gas bubble enhanced ultrasound heating in in vivo rabbit thigh. Phys Med Biol. 2003;48(2):223–241. doi:10.1088/0031-9155/48/2/306 [PubMed: 12587906]
26. Rohrer M, Bauer H, Mintorovitch J, Requardt M, Weinmann H-JJ. Comparison of magnetic properties of MRI contrast media solutions at different magnetic field strengths. Invest Radiol. 2005;40(11):715–724. doi:10.1097/01.rli.0000184756.66360.d3 [PubMed: 16230904]
27. Chen W-S, Brayman AA, Matula TJ, Crum LA. Inertial cavitation dose and hemolysis produced in vitro with or without Optison. Ultrasound Med Biol. 2003;29(5):725–737. doi:10.1016/S0301-5629(03)00013-9 [PubMed: 12754072]
28. Roberts WW, Teofilovic D, Jahnke RC, Patri J, Risdahl JM, Bertolina JA. Histotripsy of the prostate using a commercial system in a canine model. J Urol. 2014;191(3):860–865. doi:10.1016/j.juro.2013.08.077 [PubMed: 24012583]
29. Allen SP, Hernandez-Garcia L, Cain CA, Hall TL. MR-based detection of individual histotripsy bubble clouds formed in tissues and phantoms. Magn Reson Med. 2016;76(5):1486–1493. doi: 10.1002/mrm.26062 [PubMed: 26599823]
30. Vlaisavljevich E, Lin K-W, Warnez MT, et al. Effects of tissue stiffness, ultrasound frequency, and pressure on histotripsy-induced cavitation bubble behavior. Phys Med Biol. 2015;60(6):2271–2292. doi:10.1088/0031-9155/60/6/2271 [PubMed: 25715732]
31. Maxwell AD, Cain CA, Hall TL, Fowlkes JB, Xu Z. Probability of cavitation for single ultrasound pulses applied to tissues and tissue-mimicking materials. Ultrasound Med Biol. 2013;39(3):449–465. doi:10.1016/j.ultrasmedbio.2012.09.004 [PubMed: 23380152]
32. Vlaisavljevich E, Gerhardson T, Hall T, Xu Z. Effects of f-number on the histotripsy intrinsic threshold and cavitation bubble cloud behavior. Phys Med Biol. 2017;62(4):1269–1290. doi: 10.1088/1361-6560/aa54c7 [PubMed: 27995900]
33. Sukovich J, Xu Z, Kim Y, et al. Targeted Lesion Generation Through the Skull Without Aberration Correction Using Histotripsy. IEEE Trans Ultrason Ferroelectr Freq Control. 2016;63(5):671–682. doi:10.1109/TUFFC.2016.2531504 [PubMed: 26890732]
34. Duryea AP, Cain CA, Tamaddoni HA, Roberts WW, Hall TL. Removal of residual nuclei following a cavitation event using low-amplitude ultrasound. IEEE Trans Ultrason Ferroelectr Freq Control. 2014;61(10):1619–1626. doi:10.1109/TUFFC.2014.006316 [PubMed: 25265172]
35. Holmes AK, Challis RE, Wedlock DJ. A Wide Bandwidth Study of Ultrasound Velocity and Attenuation in Suspensions: Comparison of Theory with Experimental Measurements. J Colloid Interface Sci. 1993;156(2):261–268. doi:10.1006/jcis.1993.1109

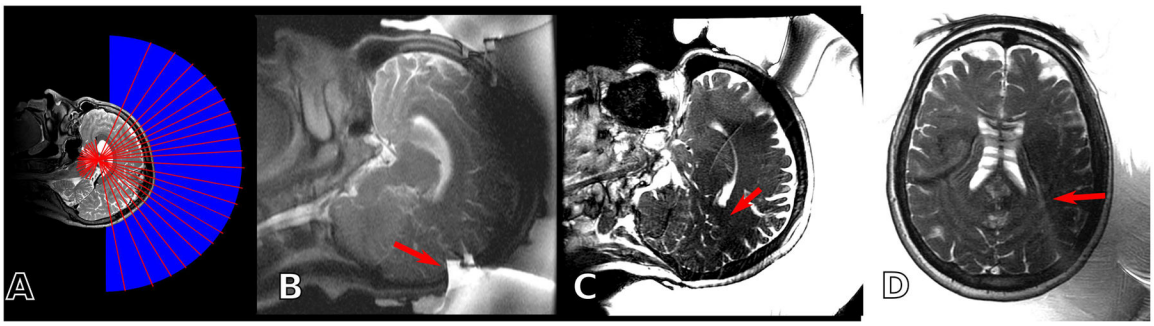

Figure 1:

(**A**) Schematic setup of a T-FUS procedure. Under MR guidance, acoustic pulses (red lines) propagate from the transducer surface, through the coupling bath (blue), and into the patient. (**B**) If the imaging field of view is too small, the large bolus of the coupling bath can alias into the anatomy of interest (red arrow). (**C**) The large MR signal of the coupling bath can skew prescan calibrations, causing sub-optimal RF calibration (red arrow). (**D**) Vibration and flow effects can cause MR signal from the coupling bath to superimpose onto the anatomy of interest (red arrow).

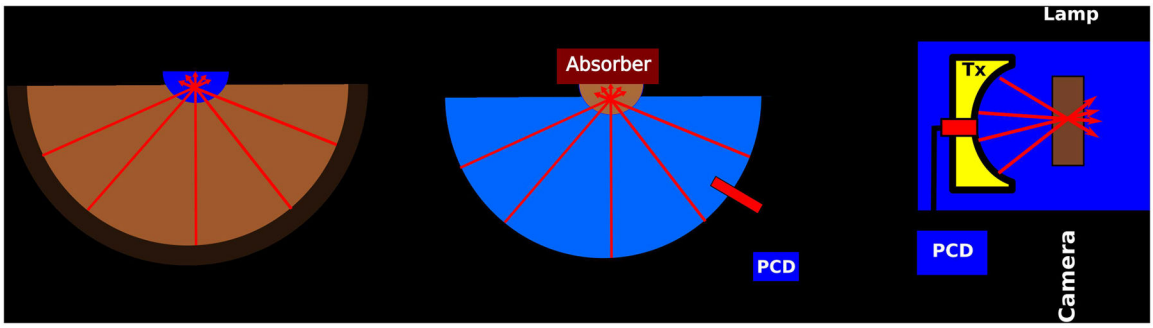

Figure 2:

(**A**) Schematic of Experiments 1 and 2. The bowl of a clinical, hemispherical transducer array was filled with various aqueous, suspended magnetite nanoparticle coupling baths and imaged by MRI. The transducer also insonated a gel target while MRI thermometry monitored thermal deposition. (**B**) Schematic of Experiment 3. The transducer in (**A**) was filled with degassed water and used to insonate various aqueous, suspended magnetite nanoparticle mixtures suspended in a small holder and backed by an acoustic absorber. PCD detectors were used to record cavitation activity. (**C**) Schematic of Experiment 4. A shock-scattering histotripsy transducer (Tx) was placed in a water tank and directly insonated various coupling baths located in an acoustically transparent holder. A high speed camera and passive cavitation detector (PCD) were used to record cavitation activity.

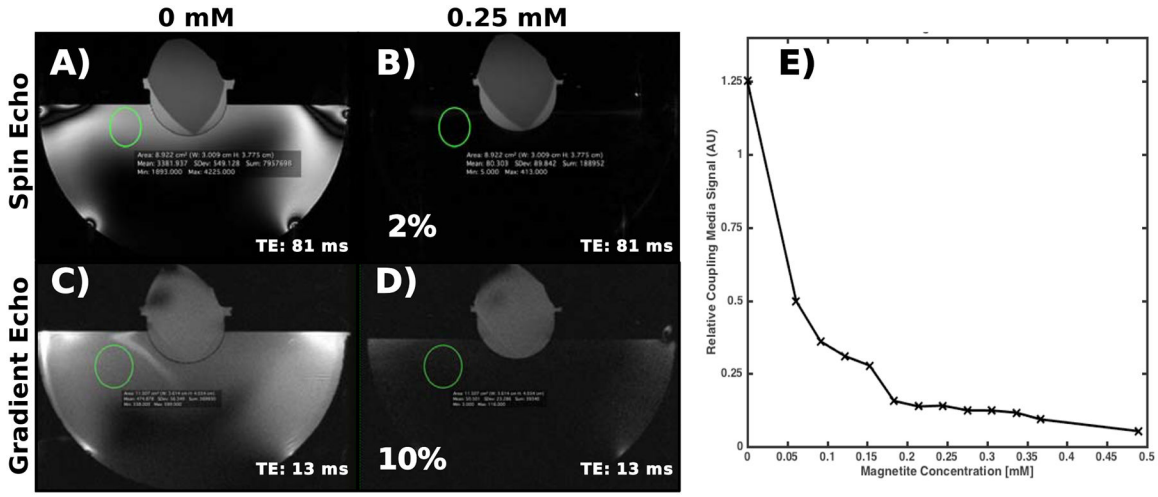

Figure 3:

(**A-D**) Example spin-echo and gradient-echo images of the gel target using two different nanoparticle concentrations in the coupling bath. The 0.25 mM nanoparticle concentration suppresses the water bath signal by 98% and 90% in the spin-echo and gradient-echo images, respectively. (**E**) Signal magnitude in the coupling bath in the turbo spin echo images relative to that of the gel as a function of nanoparticle concentration. The coupling bath signal magnitude decreases with an apparently multi-exponential curve, with the majority of signal loss occurring in the first concentration step.

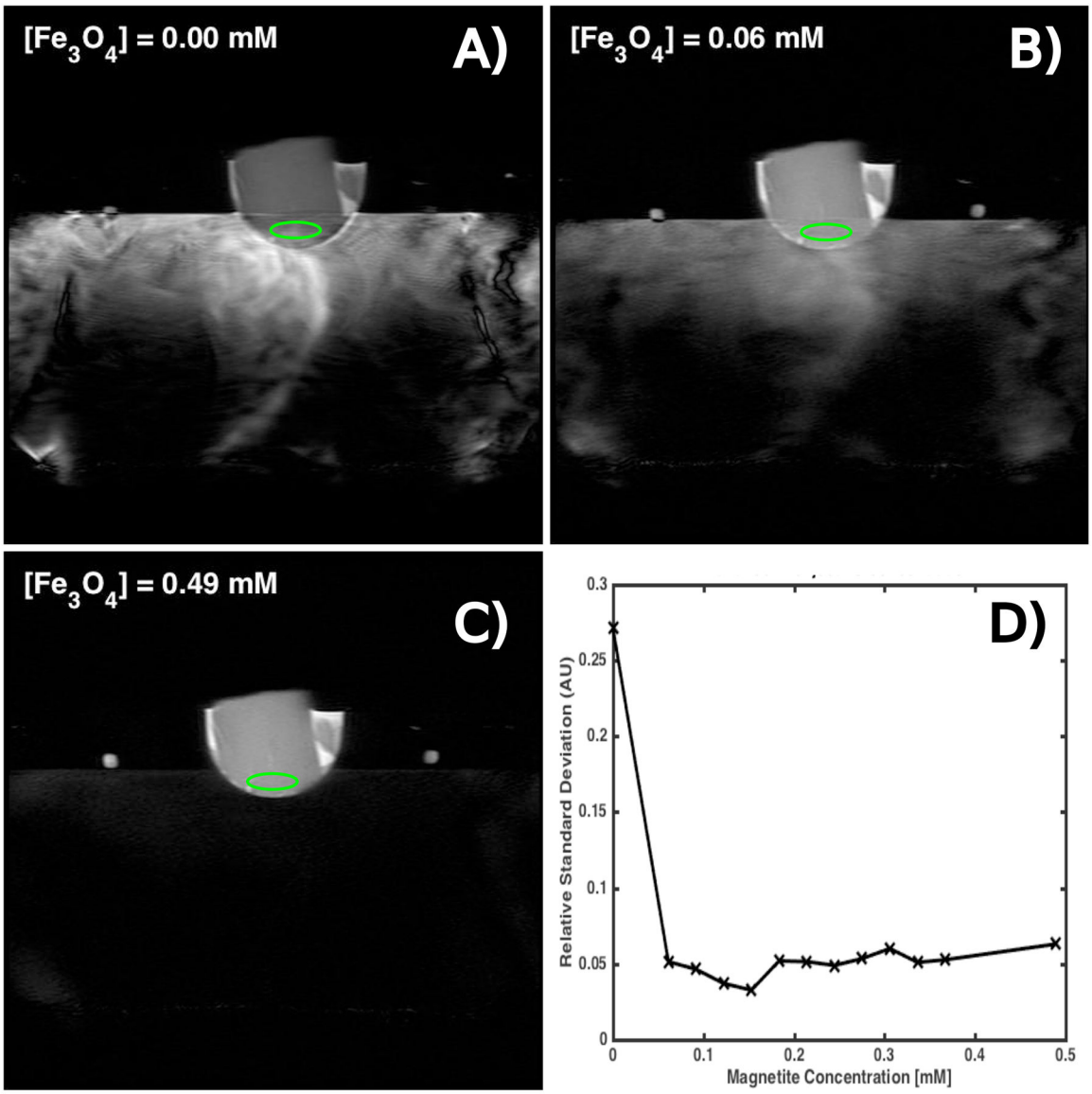

Figure 4:

(**A-C**) Example HASTE images of a homogeneous gel target in a hemispherical transducer filled with continuously circulating coupling baths containing varying concentrations of magnetite nanoparticles. Water motion causes MR signal from the coupling bath to incoherently superimpose onto the gel. (**D**) A plot of the ratio of the standard deviation of the ROI's (green ellipses). The gel is ordinarily quite homogeneous and motion artifact creates spatial fluctuations that increase the relative standard deviation in an ROI. The nanoparticles effectively suppress these fluctuations with the largest improvement caused by the first concentration increment.

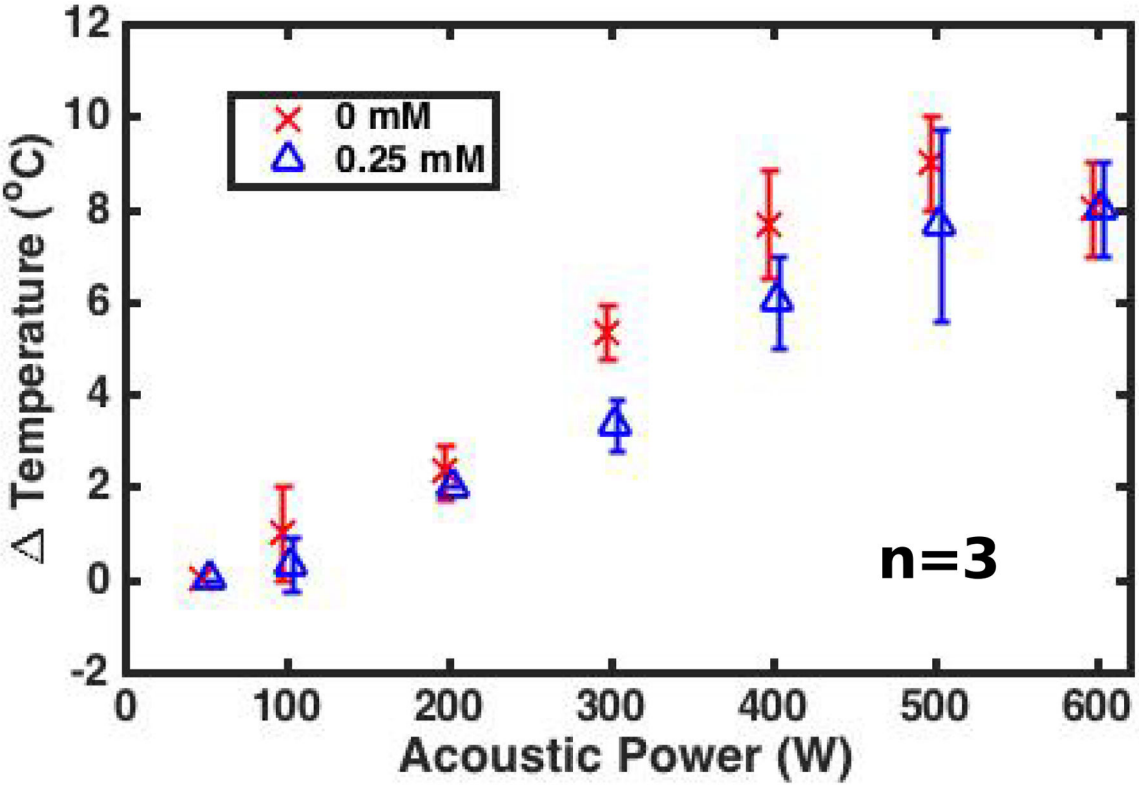

Figure 5:

Spatially averaged peak temperature change at the transducer focus in a gel target as a function of acoustic power for two coupling bath compositions. The 0.25 mM nanoparticle concentration coupling bath caused a roughly 5% decrease in peak temperature across all acoustic powers above 200 W. Data points are slightly shifted horizontally to increase figure legibility.

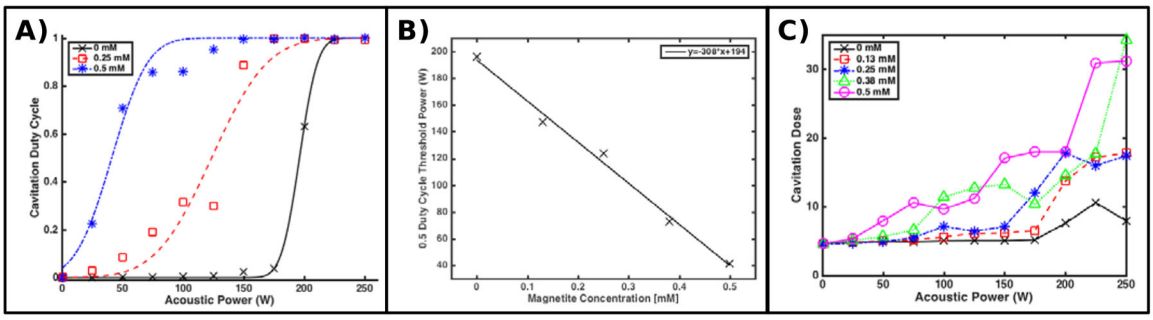

Figure 6:

(**A**) Example cavitation duty cycle curves, fit to the observed relative frequency of spectra containing cavitation emissions, observed while insonating coupling baths containing various concentrations of magnetite nanoparticles in a high duty cycle regime. (**B**) The 0.5 cavitation duty cycle threshold power, derived from all fits, including those shown in (**A**), as a function of nanoparticle concentration. This threshold decreases linearly with pressure at a rate of 308 WmM^{-1}. (**C**) Cavitation dose estimated for each acoustic power level for several coupling bath compositions. As nanoparticle concentration increases, the number and spectral power of cavitation events increases, increasing thermal dose.

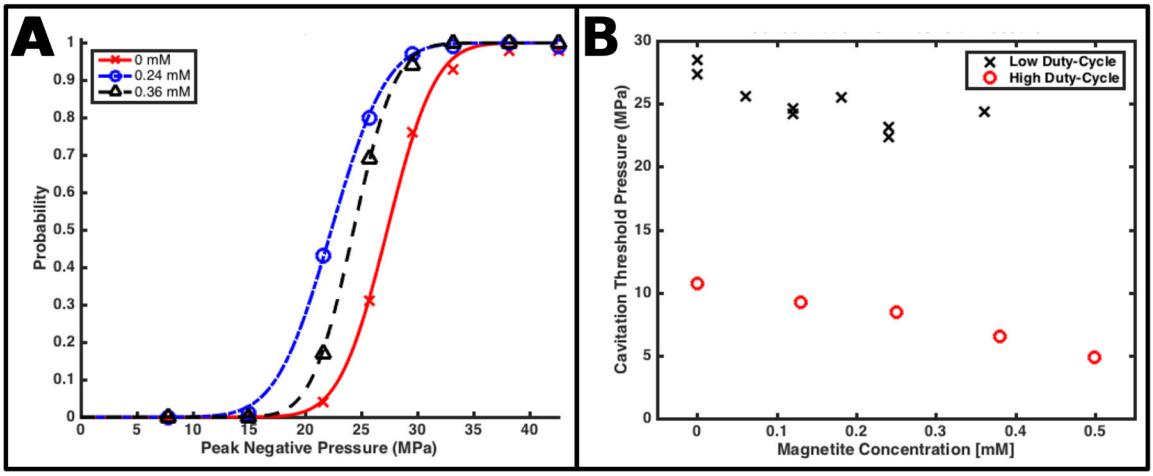

Figure 7:

(**A**) Example cavitation probability curves, fit to the relative frequency of cavitation events, as a function of peak negative pressure of acoustic pulses, observed while insonating coupling baths containing various concentrations of magnetite nanoparticles in a low duty cycle regime. (**B**) The 0.5 cavitation probability threshold pressure, derived from all fits computed from this insonation scheme, including those shown in (**A**), as a function of nanoparticle concentration. The nanoparticles reduce this threshold by 15 ± 7 %. For comparison, the high duty cycle power thresholds presented Figure 6 are converted into pressure and reproduced here.